

## Supporting Information

# Worm-like nanovector with enhanced drug loading using blends of biodegradable block copolymers

*Roxane Ridolfo<sup>†</sup>, Jeanrick J. Arends<sup>†</sup>, Jan C. M. van Hest<sup>†\*</sup>, David S. Williams<sup>‡\*</sup>*

<sup>†</sup>Bio-Organic Chemistry, Institute for Complex Molecular Systems, Eindhoven University of Technology, P.O. Box 513 (STO 3.41), 5600 MB Eindhoven, The Netherlands

<sup>‡</sup>Department of Chemistry, College of Science, Swansea University, Swansea, United Kingdom

### Corresponding Authors

\*E-mail: [d.s.williams@swansea.ac.uk](mailto:d.s.williams@swansea.ac.uk)

\*E-mail: [j.c.m.v.hest@tue.nl](mailto:j.c.m.v.hest@tue.nl)

## INSTRUMENTATION

**Nuclear Magnetic Resonance spectroscopy (NMR):** Proton ( $^1\text{H}$ ) and Carbon ( $^{13}\text{C}$ ) NMR spectra were recorded on a Bruker Avance 400 MHz spectrometer with  $\text{CDCl}_3$  as a solvent and TMS as internal standard. Chemical shifts were reported as  $\delta$  values (ppm) and coupling constants J were reported in Hz.  $^{13}\text{C}$ -NMR spectra were proton decoupled.

**Gel permeation chromatography (GPC):** GPC was conducted using a Shimadzu Prominence-i GPC system with a PL gel 5  $\mu\text{m}$  mixed D column (Polymer Laboratories) with a differential refractive index detector and THF as an eluent, with a flow rate of 1 mL/min. Molar Mass distributions were calculated using polystyrene standards. Samples were prepared in THF at a concentration of 1 mg/mL.

**Differential Scanning Calorimetry (DSC):** Thermal properties were measured on a DSC Q2000 from TA instruments and raw data processed with TA universal analysis 2000 software. Approximately 10 mg of sample was analyzed in a 50  $\mu\text{L}$  Tzero aluminum hermetic pan. Thermal measurements consisted out of two full heating and cooling cycles within a temperature range of  $[-80\text{ }^\circ\text{C} ; 80\text{ }^\circ\text{C}]$ , a heating and cooling ramp of  $10\text{ }^\circ\text{C}$  per minute was used.

**Dynamic light scattering and Zeta-potential measurements (DLS & Z-P):** DLS and Z-P measurements were conducted using a Malvern Instruments Zetasizer Nano (ZSP), with Zetasizer Software (Malvern Instruments) used for processing and analyzing data. Measurements were all performed at room temperature unless otherwise stated. To register Z-P values, a 1mL DTS1070 capillary cell was used.

**Cryogenic transmission electron microscopy (cryo-TEM):** Samples for Cryo-TEM measurements were prepared by first treating the grids (Quantifoil R2/2 Cu 200 mesh grids or

Lacey carbon coated, R2/2, Cu, 200 mesh, EM sciences) in a Cressington 208 carbon coater for 40 seconds. Afterwards, 3  $\mu$ L of sample solution was brought on the grid and blotted in a FEI Vitrobot Mark III, at 100 % humidity for 3 seconds (offset -3) and directly plunged in liquid ethane. TEM imaging was performed using a FEI Titan (300 kV electron source) with a LaB6 filament and equipped with an autoloader station. Analysis and processing of the data was performed using ImageJ, a program developed by the NIH and available as public domain software at <http://rsbweb.nih.gov/ij/>.

**Asymmetric Flow Field-Flow Fractionation (AF4), multi-angle light scattering (MALS) and dynamic light scattering (DLS):** AF4-MALS-DLS experiments were performed on a Wyatt Eclipse Dualtec instrument connected to a Shimadzu LC-20A Prominence system with Shimadzu CTO20A injector. The following detectors were connected to AF4: a Shimadzu SPD20A UV detector; a Wyatt DAWN HELEOS II light scattering detector (MALS) installed at different angles (12.9°, 20.6°, 29.6°, 37.4°, 44.8°, 53.0°, 61.1°, 70.1°, 80.1°, 90.0°, 99.9°, 109.9°, 120.1°, 130.5°, 149.1°, and 157.8°) using a laser operating at 664.5 nm; a DLS detector installed at an angle of 140.1° and a Wyatt Optilab Rex refractive index detector. Detectors were normalized using Bovine Serum Albumin. The processing and analysis of the LS data and radius of gyration ( $R_G$ ) calculations were performed on Astra 7.1.2 software (using the Berry model). All AF4 fractionations were performed on an AF4 short channel with regenerated cellulose (RC) 10 kDa membrane (Millipore) and spacer of 350  $\mu$ m.

**UV-VIS and Fluorescence spectroscopy:** Drug loading assays were performed in a Helma Analytics High Precision Cell made of Quartz SUPRASIL on a Jasco V-750 spectrophotometer possessing a multi-cell holder PAC-743. Parameters for UV-VIS experiments were: Mode Absorbance, Range 220-260 nm, Interval 2 nm, Bandwidth 1nm, Response 0.24 s, Scan Speed

100 nm/min. CMC assays were performed in a Black Chimney 96-well plate on a Tecan Spark M10 plate reader. Parameters for CMC measurements were: mode fluorescence intensity, excitation wavelength 360 nm, emission wavelength 485 nm, gain 60, mirror 50 %, 30 flashes and z-position 20000  $\mu\text{m}$ . All experiments were led at  $25 \pm 0.5$  °C.

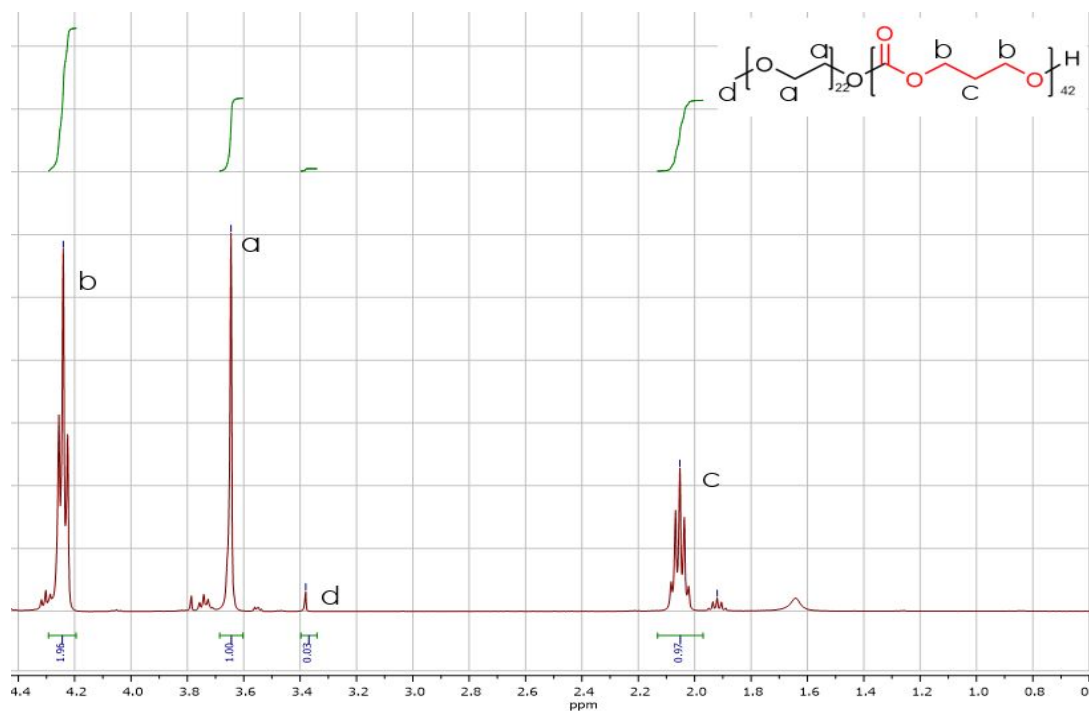
**Microscopy:** Microscopy images were performed using a Leica TCS SP8 STED 3X CW 3D microscope.

**Flow cytometry:** All FACS measurements were done using a FACS Aria III equipped with a 70 $\mu\text{m}$  nozzle. Hoechst33342 was excited by a 405 nm laser and detected through a 450/65 bandpass filter with a PMT voltage of 297 mV. Bodipy-FL was excited by a 488 nm laser and detected through a 530/30 bandpass filter with a PMT voltage of 506 mV. For all analyses, doublet cells were excluded by standard doublet discrimination with forward- and side scatter area versus height plots. No spectral interference was observed between Hoechst and Bodipy-FL, therefore, no compensation was necessary. All samples were recorded with a flow rate of 8.0 mL/min. Data was displayed using FlowJo software (v10).

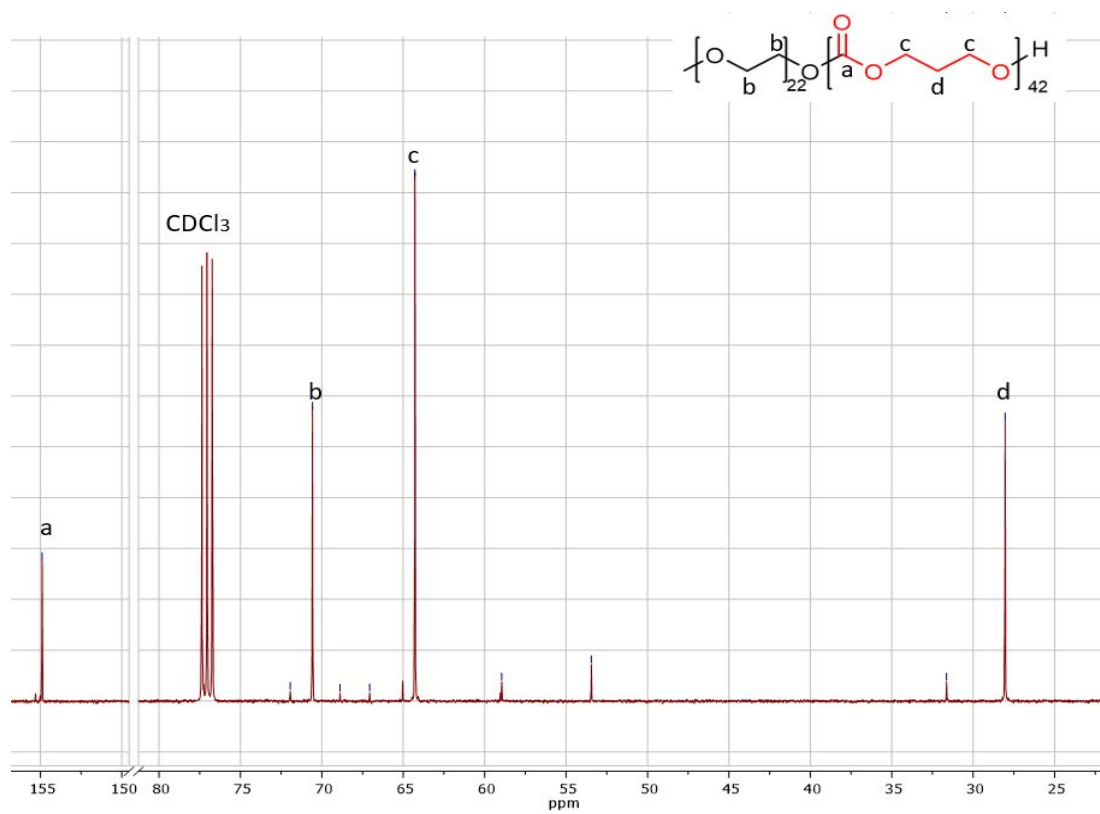
**Supplementary Figure 1.** Synthesis and characterization of poly(ethylene glycol)-poly(trimethylene carbonate -g-  $\epsilon$ -caprolactone) block copolymers



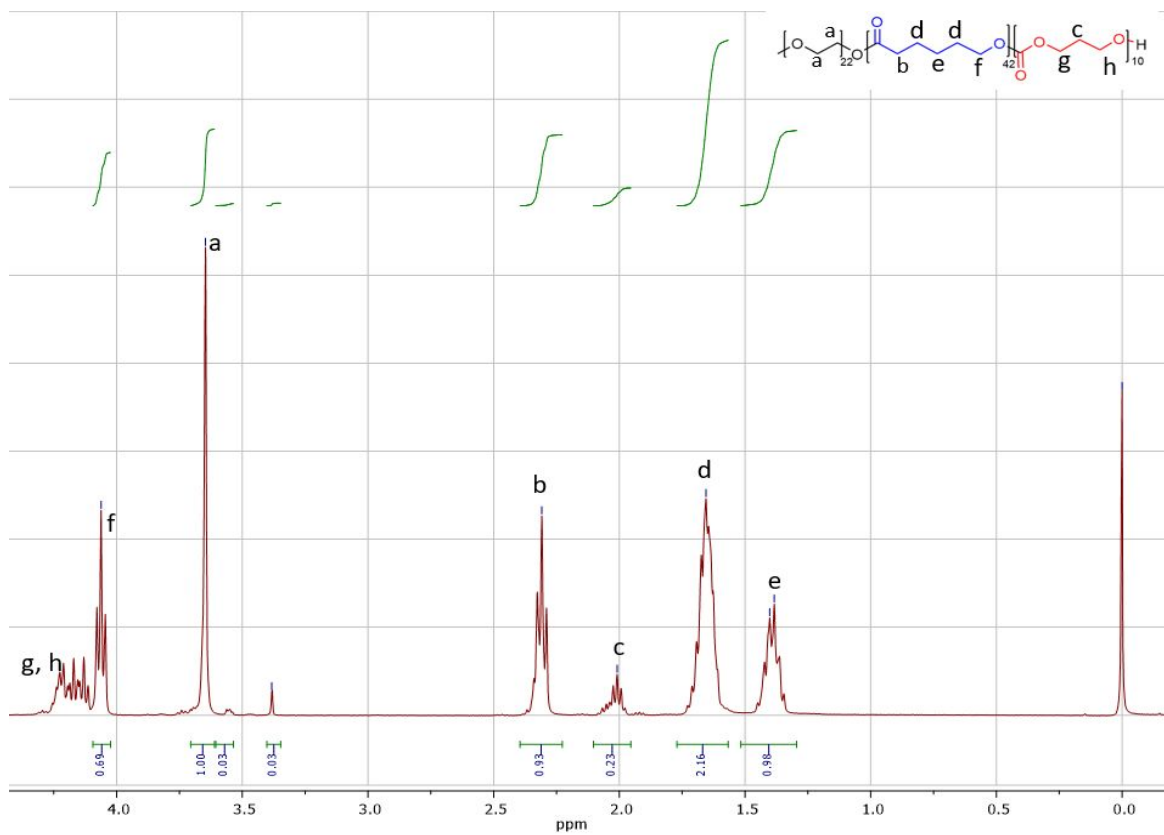
Synthetic Scheme



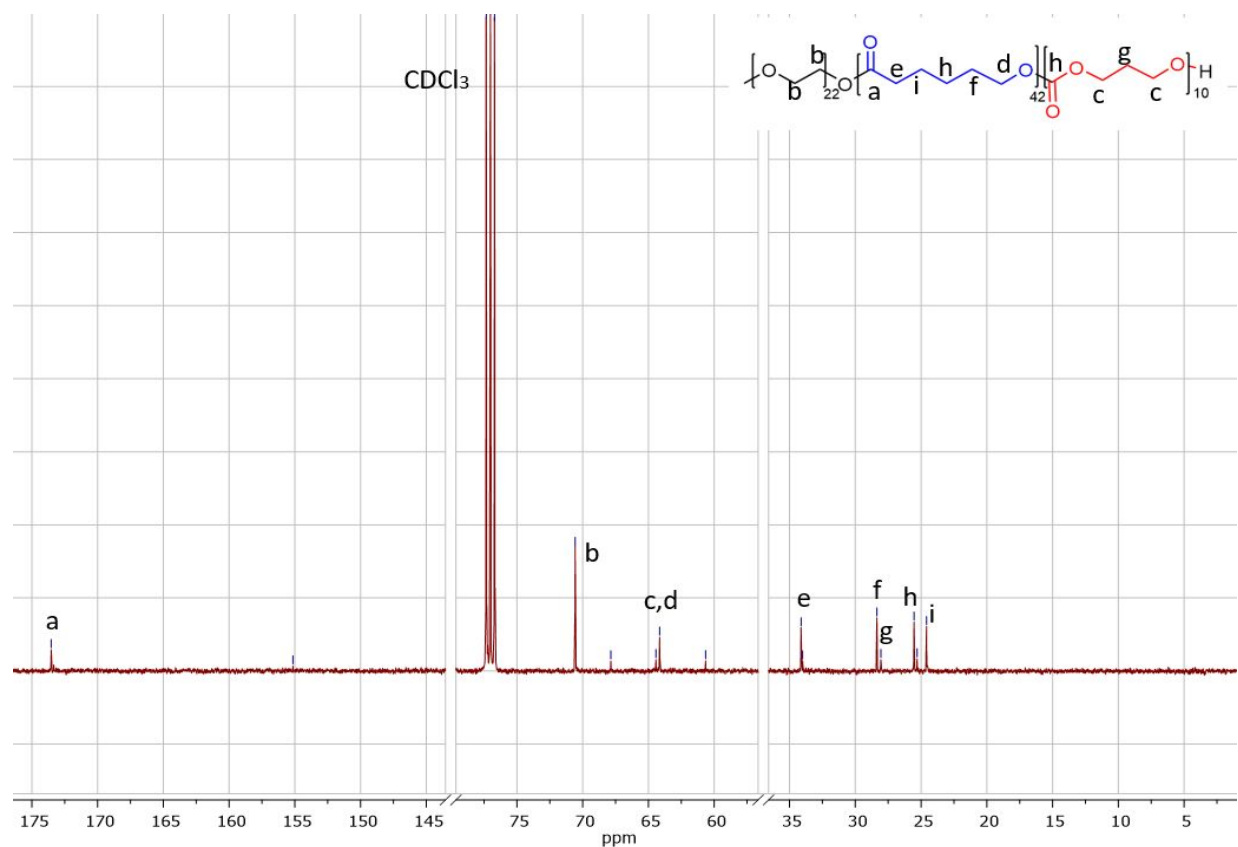
$^1\text{H}$ -NMR (400 MHz,  $\text{CDCl}_3$ ):  $\delta$  4.24 (t, 4H x 42,  $J = 6.42$  Hz,  $-\text{O}-\text{CH}_2-\text{CH}_2-\text{CH}_2-\text{O}$ , TMC), 3.64 (s, 4H x 22,  $-\text{O}-\text{CH}_2-\text{CH}_2-\text{O}$ , Me-PEG-OH), 3.38 (s, 3H,  $\text{CH}_3$ -PEG-O-), 2.05 (m, 2H x 42,  $J = 6.10$  Hz,  $-\text{O}-\text{CH}_2-\text{CH}_2-\text{CH}_2-\text{O}$ , TMC).



$^{13}\text{C-NMR}$  (100 Mhz,  $\text{CDCl}_3$ ),  $\delta$  154.80 (-O-CO-O-, carbonate ester), 70.57 ( $\text{CH}_3\text{-(O-CH}_2\text{-CH}_2\text{-CH}_2\text{)}_{22}\text{-O-}$ ), 64.28 (-O-CH<sub>2</sub>-CH<sub>2</sub>-CH<sub>2</sub>-O-), 28.04 (-O-CH<sub>2</sub>-CH<sub>2</sub>-CH<sub>2</sub>-O-).



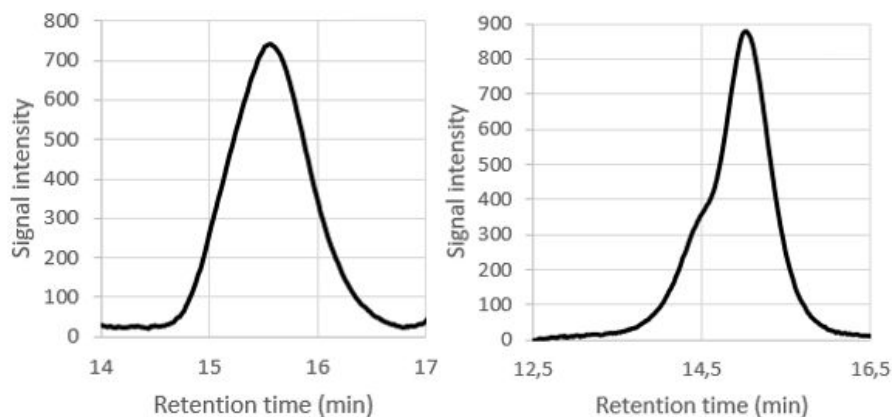
<sup>1</sup>H-NMR (400 MHz, CDCl<sub>3</sub>): δ=4.06ppm (t, -O-(CH<sub>2</sub>)<sub>4</sub>-CH<sub>2</sub>-O-TMC, ε-CL), 3.65ppm (s, -O-CH<sub>2</sub>-CH<sub>2</sub>-O-, Me-PEG-OH), 3.38ppm (s, CH<sub>3</sub>-, Me-PEG-OH), 2.31ppm (m, CO-CH<sub>2</sub>-(CH<sub>2</sub>)<sub>4</sub>-O-, ε-CL), 2.01ppm (m, -O-CH<sub>2</sub>-CH<sub>2</sub>-CH<sub>2</sub>-O, TMC), 1.66ppm (m, -O-CH<sub>2</sub>-CH<sub>2</sub>-CH<sub>2</sub>-CH<sub>2</sub>-CH<sub>2</sub>-O, ε-CL), 1.38ppm (m, -O-CH<sub>2</sub>-CH<sub>2</sub>-CH<sub>2</sub>-CH<sub>2</sub>-CH<sub>2</sub>-O, ε-CL).



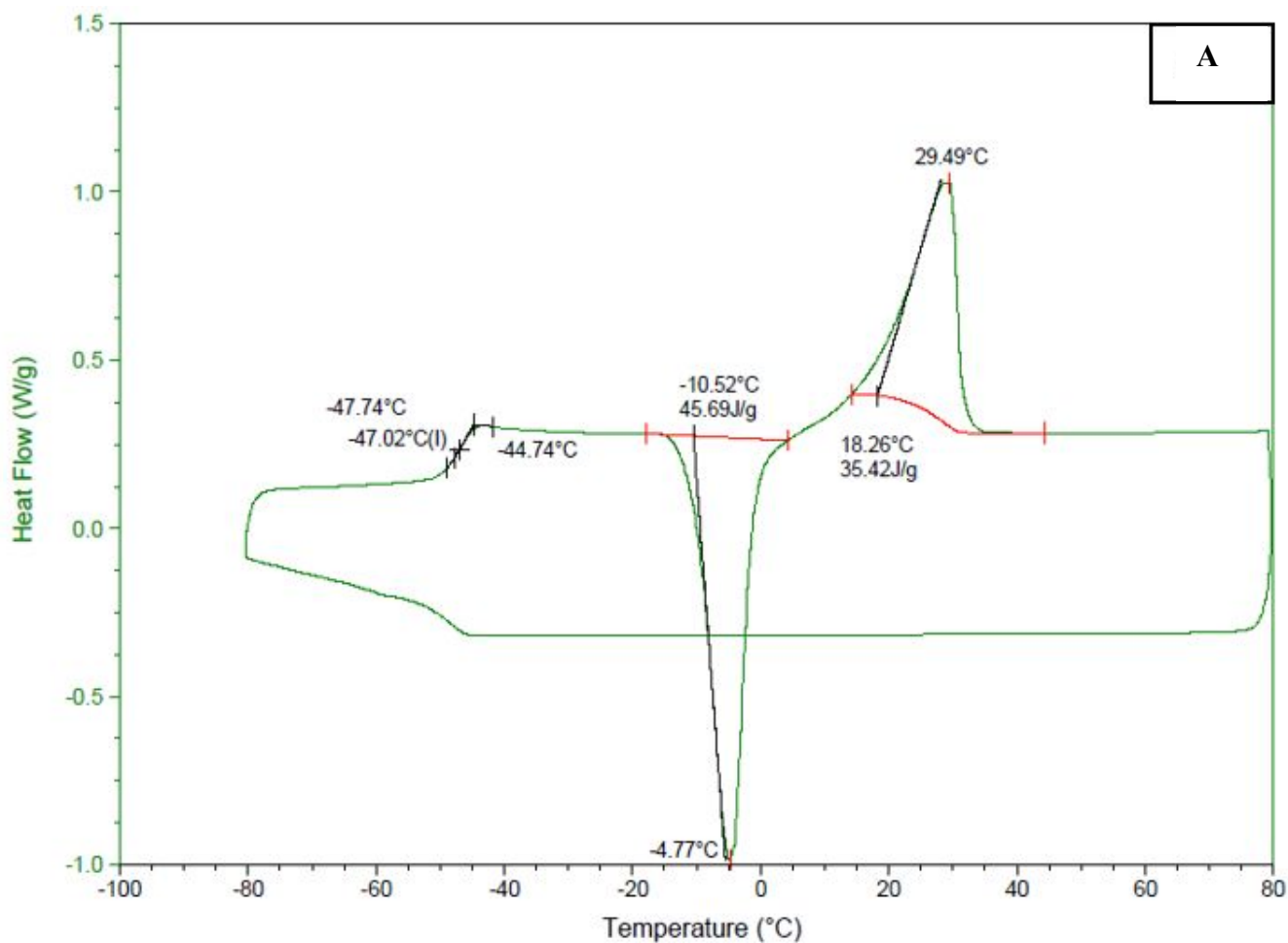
<sup>13</sup>C-NMR (100 MHz, CDCl<sub>3</sub>): δ=173.53ppm (C=O, ε-CL), 155.15ppm (-O-CO-O-, TMC), 70.57ppm (-O-CH<sub>2</sub>-CH<sub>2</sub>-O-, Me-PEG-OH), 64.15ppm (-O-CH<sub>2</sub>-CH<sub>2</sub>-CH<sub>2</sub>-O-CO-CH<sub>2</sub>-(CH<sub>2</sub>)<sub>4</sub>-O-, TMC, ε-CL), 34.01ppm (-CO-(CH<sub>2</sub>)<sub>4</sub>-CH<sub>2</sub>-O-, ε-CL), 28.36ppm (-CO-CH<sub>2</sub>-CH<sub>2</sub>-(CH<sub>2</sub>)<sub>3</sub>-O-, ε-CL), 28.06ppm (-CO-CH<sub>2</sub>-CH<sub>2</sub>-CH<sub>2</sub>-OC-, TMC), 25.54ppm (CO-CH<sub>2</sub>-CH<sub>2</sub>-CH<sub>2</sub>-CH<sub>2</sub>-CH<sub>2</sub>-O-, ε-CL), 24.62ppm (CO-(CH<sub>2</sub>)<sub>3</sub>-CH<sub>2</sub>-CH<sub>2</sub>-O-, ε-CL).



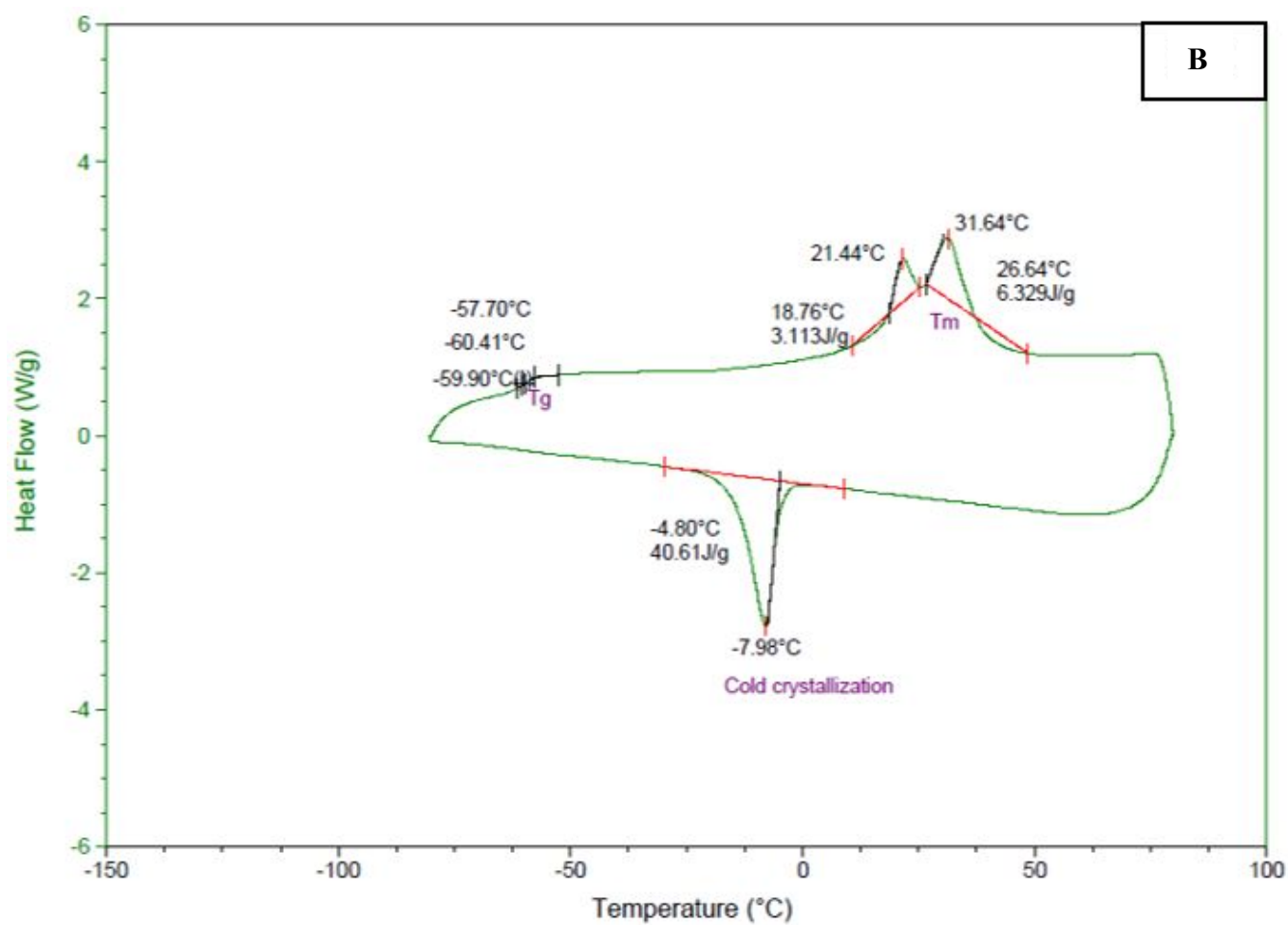
**Supplementary Figure 2.** GPC traces of the H<sub>3</sub>C-PEG<sub>22</sub>-b-PTMC<sub>42</sub> (left) and H<sub>3</sub>C-PEG<sub>22</sub>-b-p(CL<sub>42</sub>-g-TMC<sub>11</sub>) (right) block copolymers. The y-axis shows the intensity of the dRI signal.



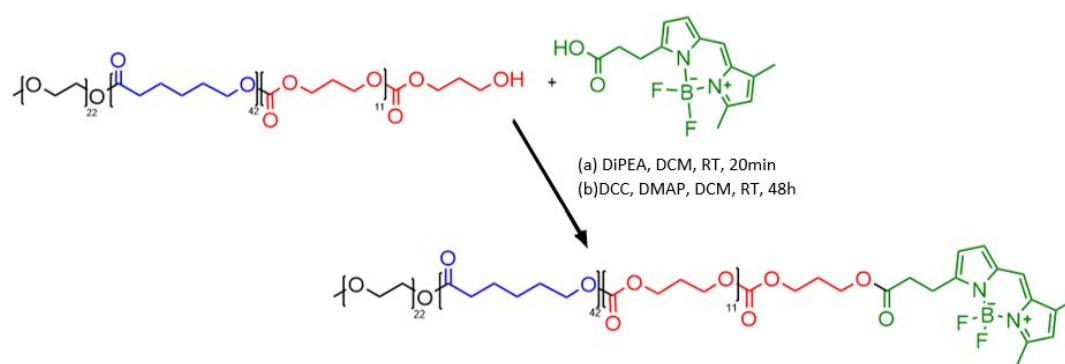
**Supplementary Figure 3.** DSC of H<sub>3</sub>C-PEG<sub>22</sub>-b-PTMC<sub>42</sub> (A) and H<sub>3</sub>C-PEG<sub>22</sub>-b-p(CL<sub>42</sub>-g-TMC<sub>11</sub>) (B)



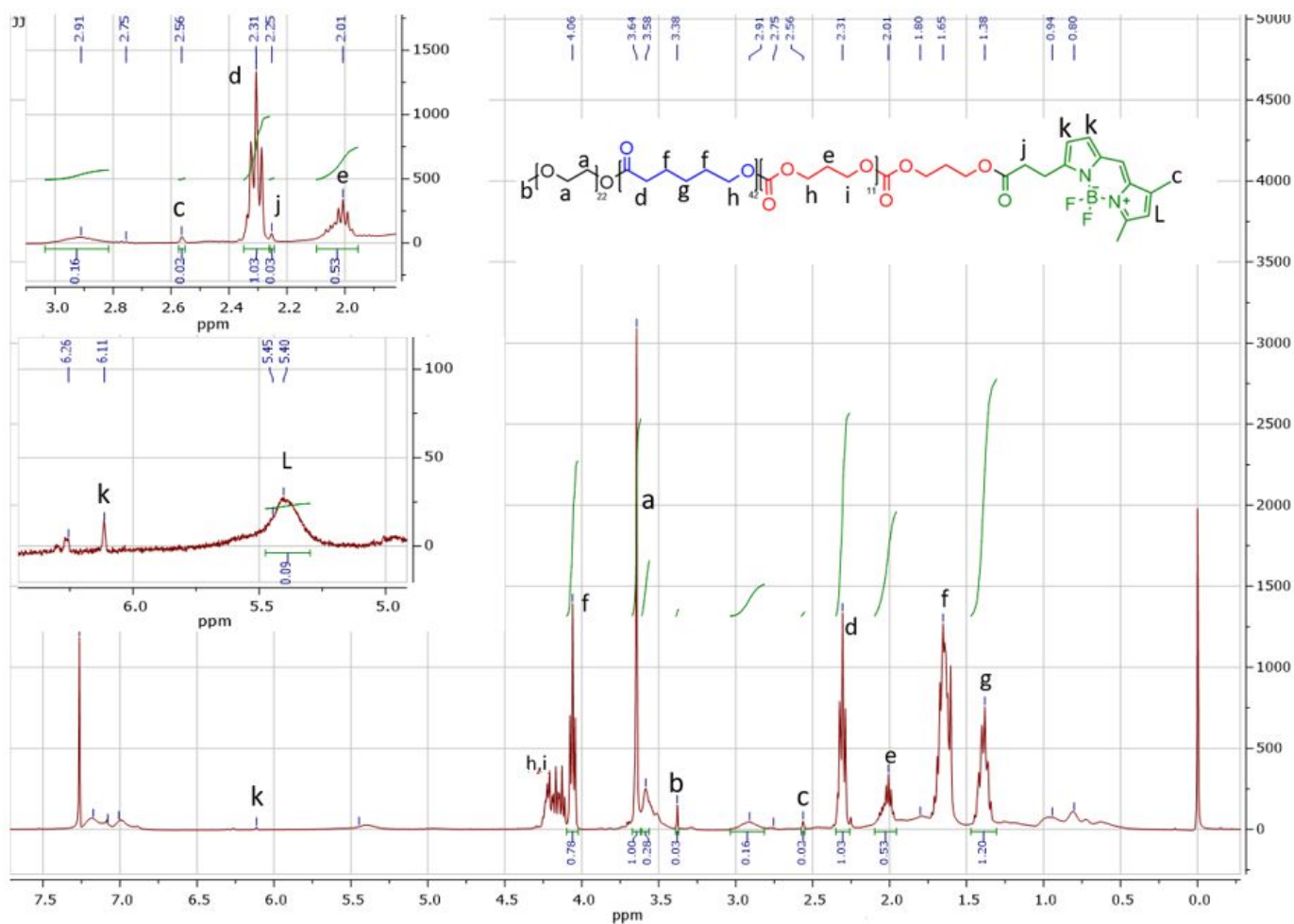
B



**Supplementary Figure 4.** Coupling of BODIPY-FL-CO<sub>2</sub>H dye to H<sub>3</sub>C-PEG22-b-p(CL42-g-TMC11)

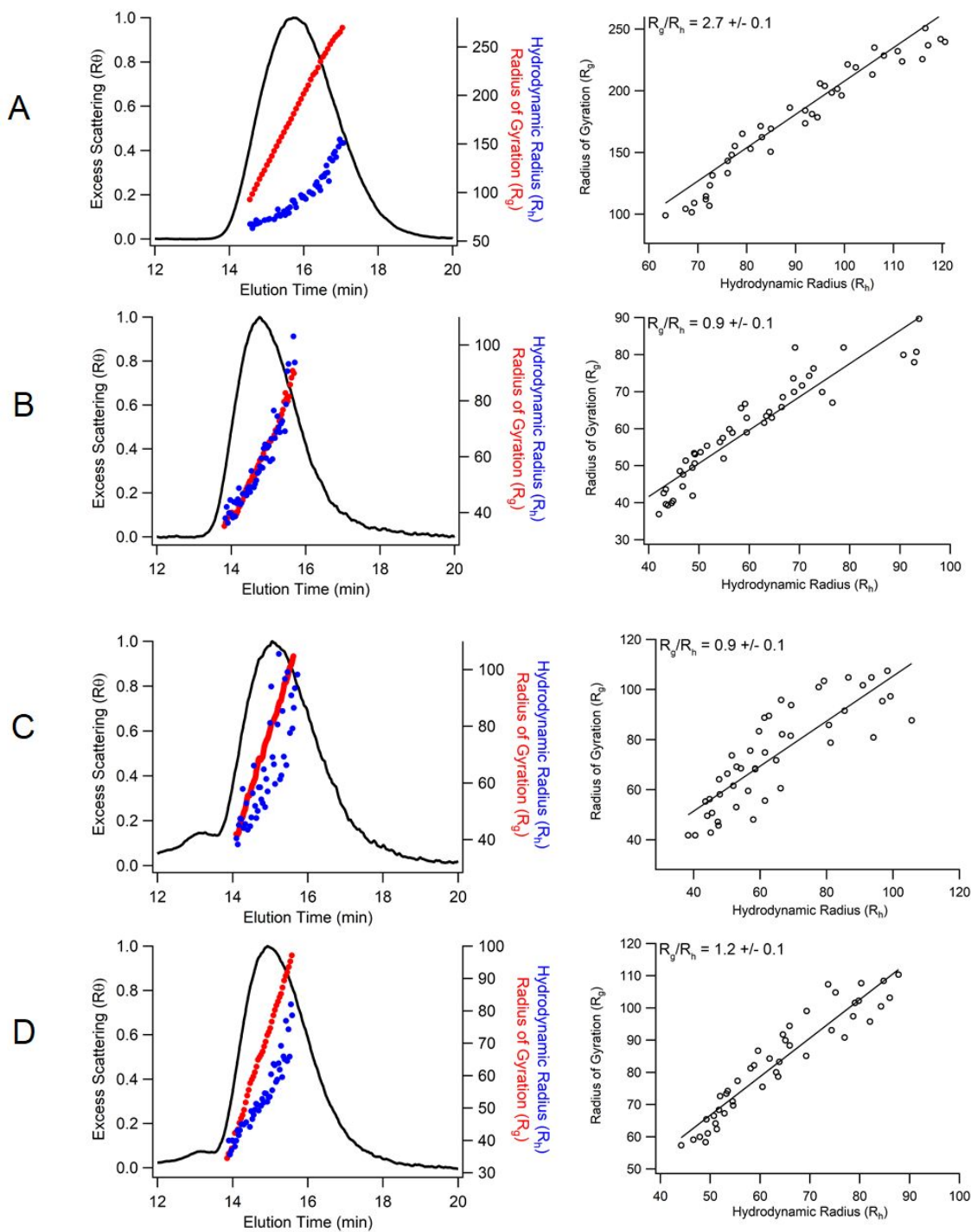


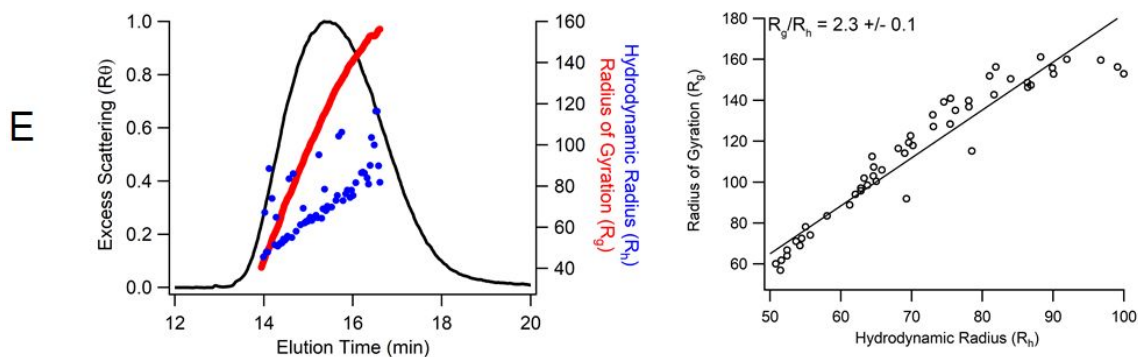
Synthetic Scheme



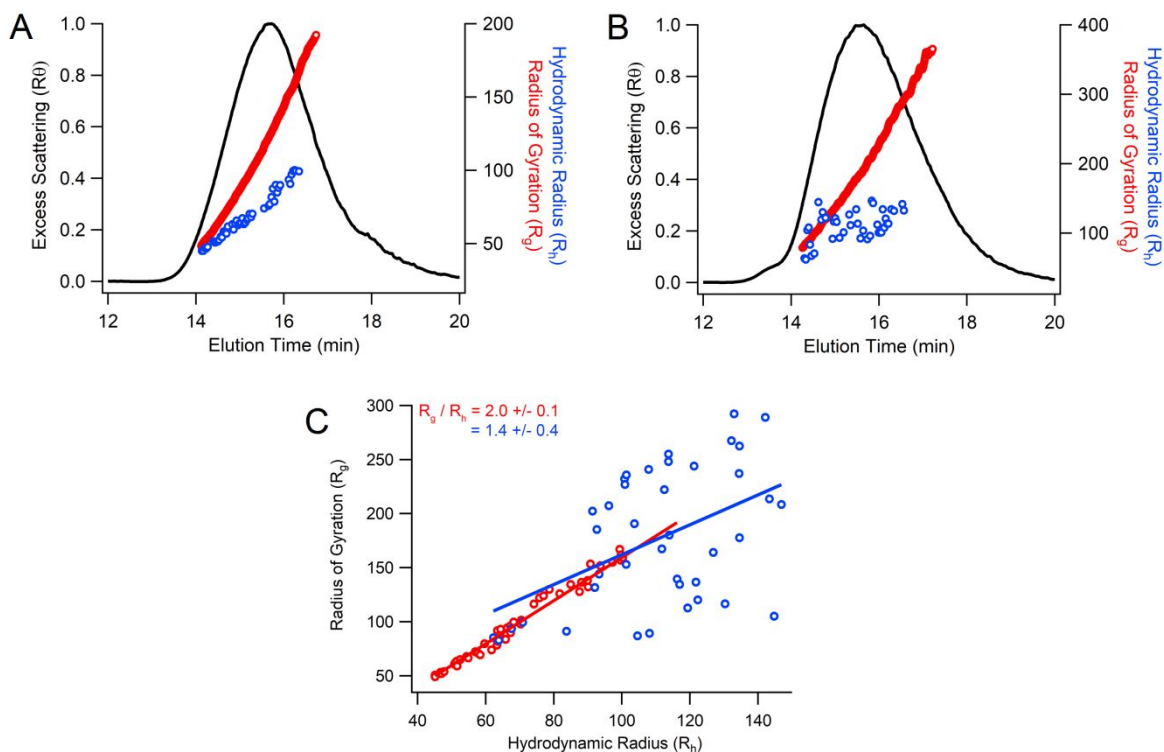
<sup>1</sup>H-NMR (400MHz, CDCl<sub>3</sub>): δ= 6.11ppm(s, BDP-FL), 5.40ppm (s, BDP-FL), 4.06ppm (t, -O-(CH<sub>2</sub>)<sub>4</sub>-CH<sub>2</sub>-O-TMC, ε-CL), 3.64ppm (s, -O-CH<sub>2</sub>-CH<sub>2</sub>-O-, HOOC-PEG-O-), 3.38ppm (CH<sub>3</sub>-PEG<sub>22</sub>-O-), 2.56ppm, (s, -CH<sub>3</sub>, BDP FL), 2.31ppm (m, CO-CH<sub>2</sub>-(CH<sub>2</sub>)<sub>4</sub>-O-, ε-CL), 2.25ppm (t, OC-CH<sub>2</sub>, BDP-FL), 2.01ppm (m, -O-CH<sub>2</sub>-CH<sub>2</sub>-CH<sub>2</sub>-O-, TMC), 1.65ppm (m, -O-CH<sub>2</sub>-CH<sub>2</sub>-CH<sub>2</sub>-CH<sub>2</sub>-O-, ε-CL), 1.38ppm (m, -O-CH<sub>2</sub>-CH<sub>2</sub>-CH<sub>2</sub>-CH<sub>2</sub>-O-, ε-CL).

**Supplementary Figure 5.** Asymmetric Flow Field-Flow Fractionation (AF4) data for formulation 1-5 (Fig.1) recording the shape factor ( $\rho = R_g/R_h$ ) using in-line multi-angle light scattering (MALS) and DLS. (A)-(E) respectively formulations 1-5.

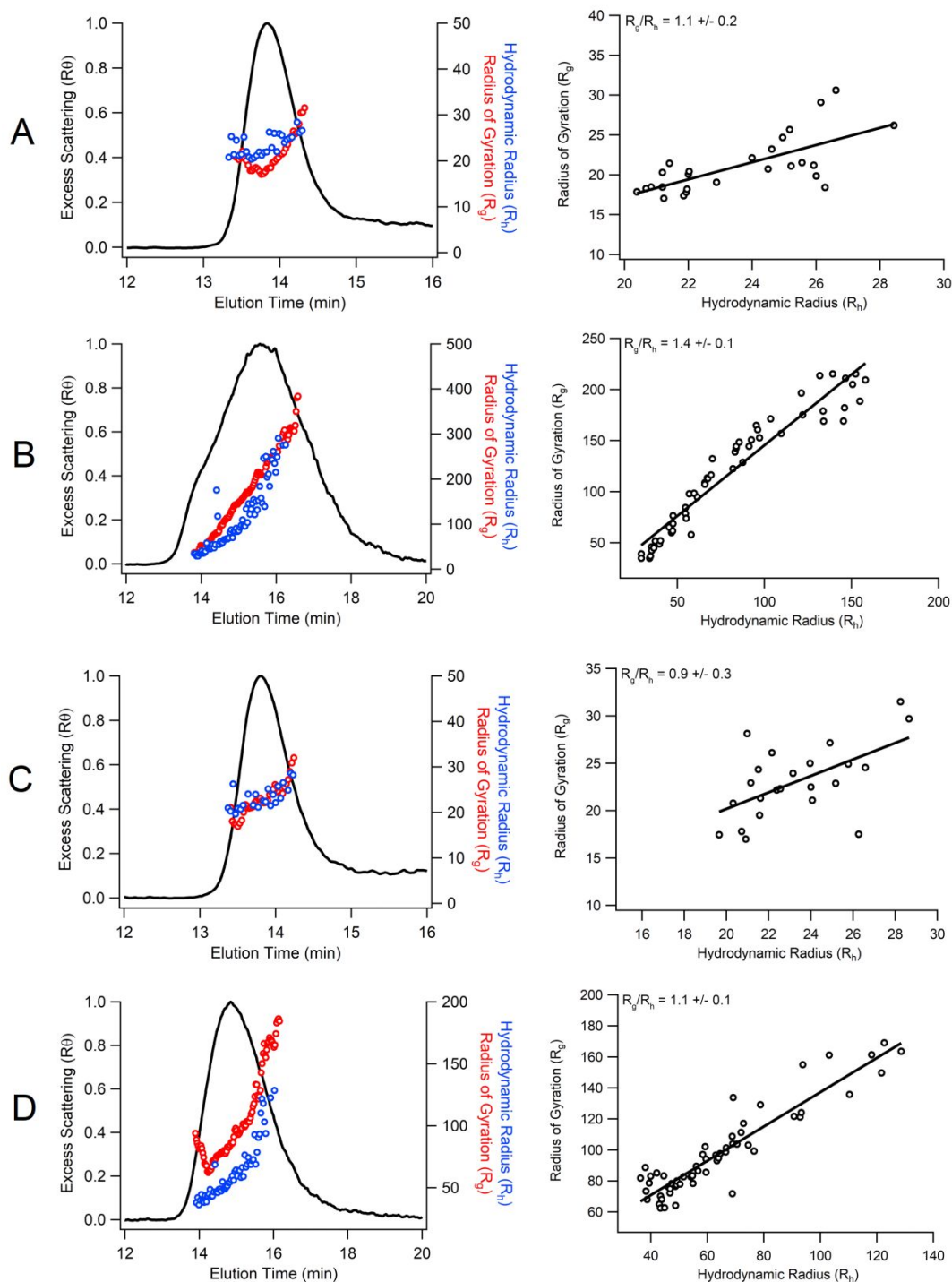




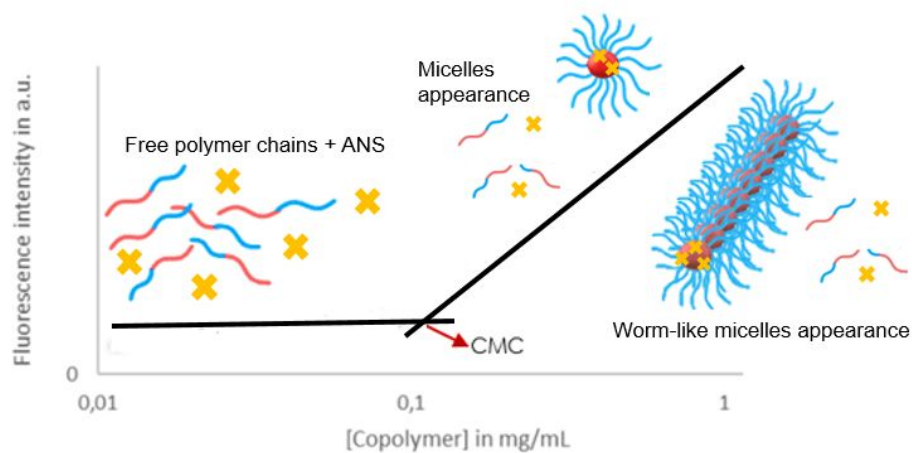
**Supplementary Figure 6.** Asymmetric Flow Field-Flow Fractionation (AF4) data for buffer effect on formulation 6 recording the shape factor ( $\rho = R_g/R_h$ ) using in-line multi-angle light scattering (MALS) and DLS. (A) PBS, (B) water, (C) Red= PBS, Blue= water.



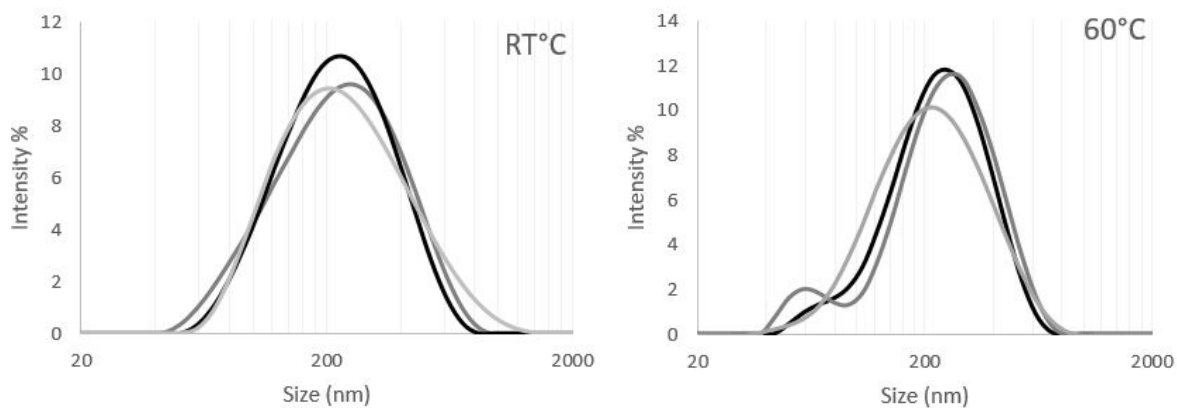
**Supplementary Figure 7.** Asymmetric Flow Field-Flow Fractionation (AF4) data for formulation 1-4 (Fig.2A) recording the shape factor ( $\rho = R_g/R_h$ ) using in-line multi-angle light scattering (MALS) and DLS. (A)-(D) respectively formulations 1-4.



**Supplementary Figure 8.** Illustration of typical graphic for CMC determination

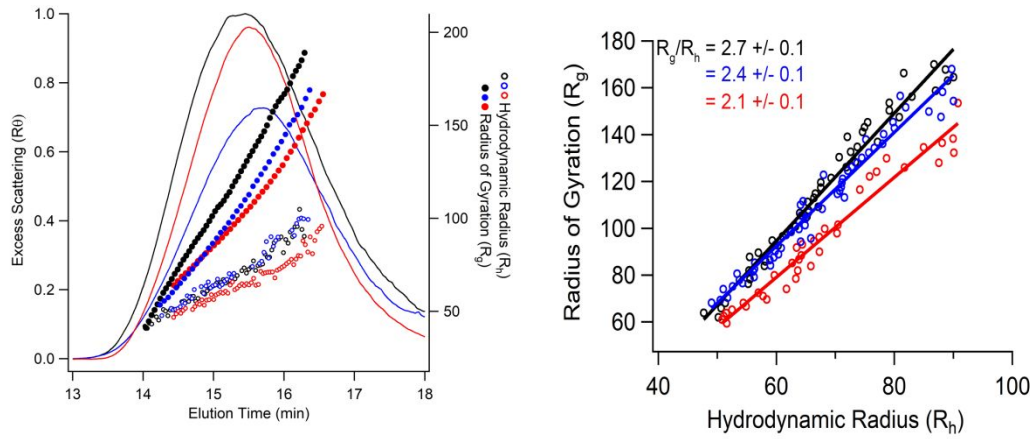


**Supplementary Figure 9.** Size distribution by intensity (DLS) data for temperature effect on formulation 6 (3 curves for 3 repetitions)



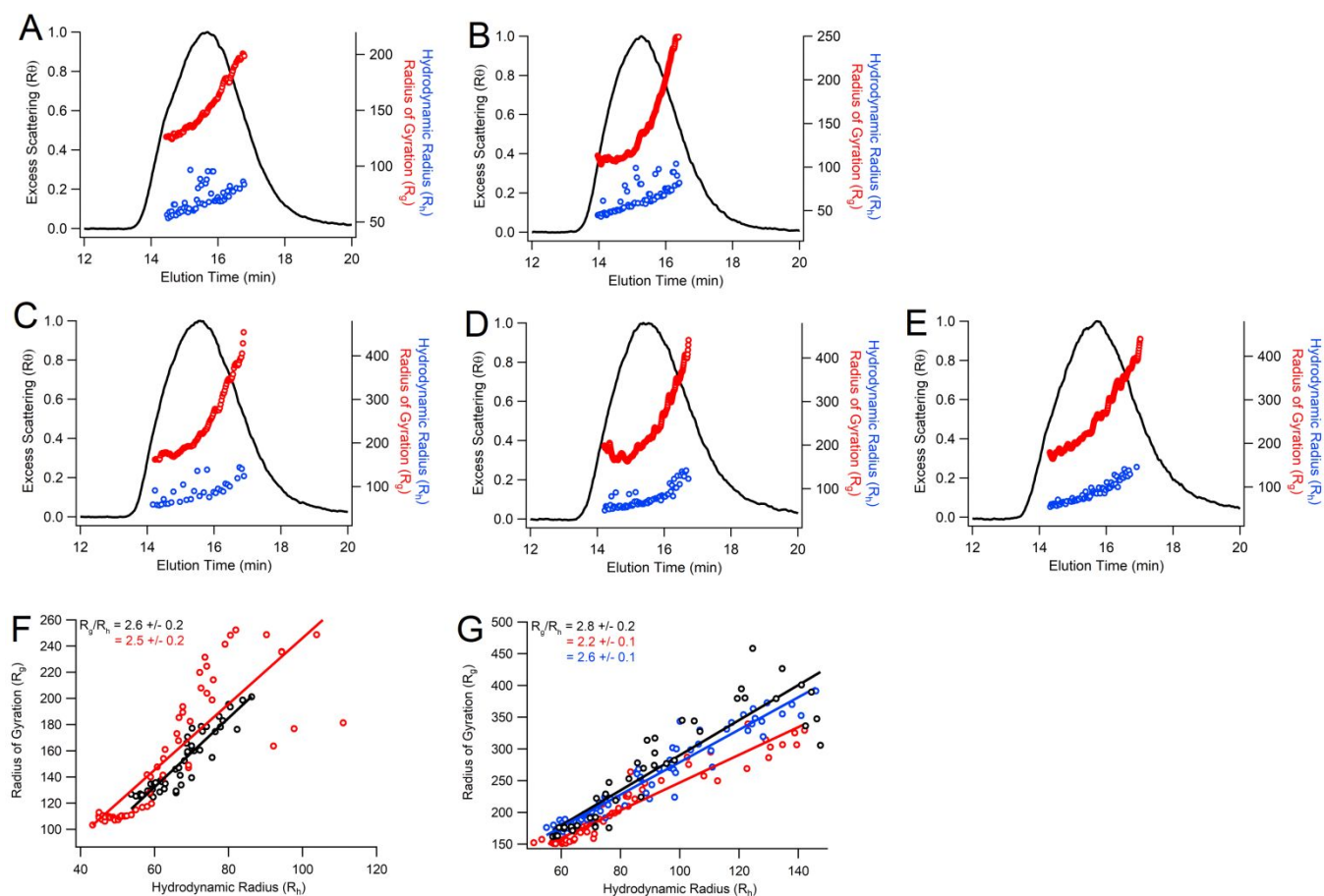


**Supplementary Figure 10.** Asymmetric Flow Field-Flow Fractionation (AF4) data for overtime stability formulations at different time points recording the shape factor ( $\rho = R_g/R_h$ ) using in-line multi-angle light scattering (MALS) and DLS. Black= original sample 6, blue= after 5 months at room temperature, red= after 5 months in the fridge.

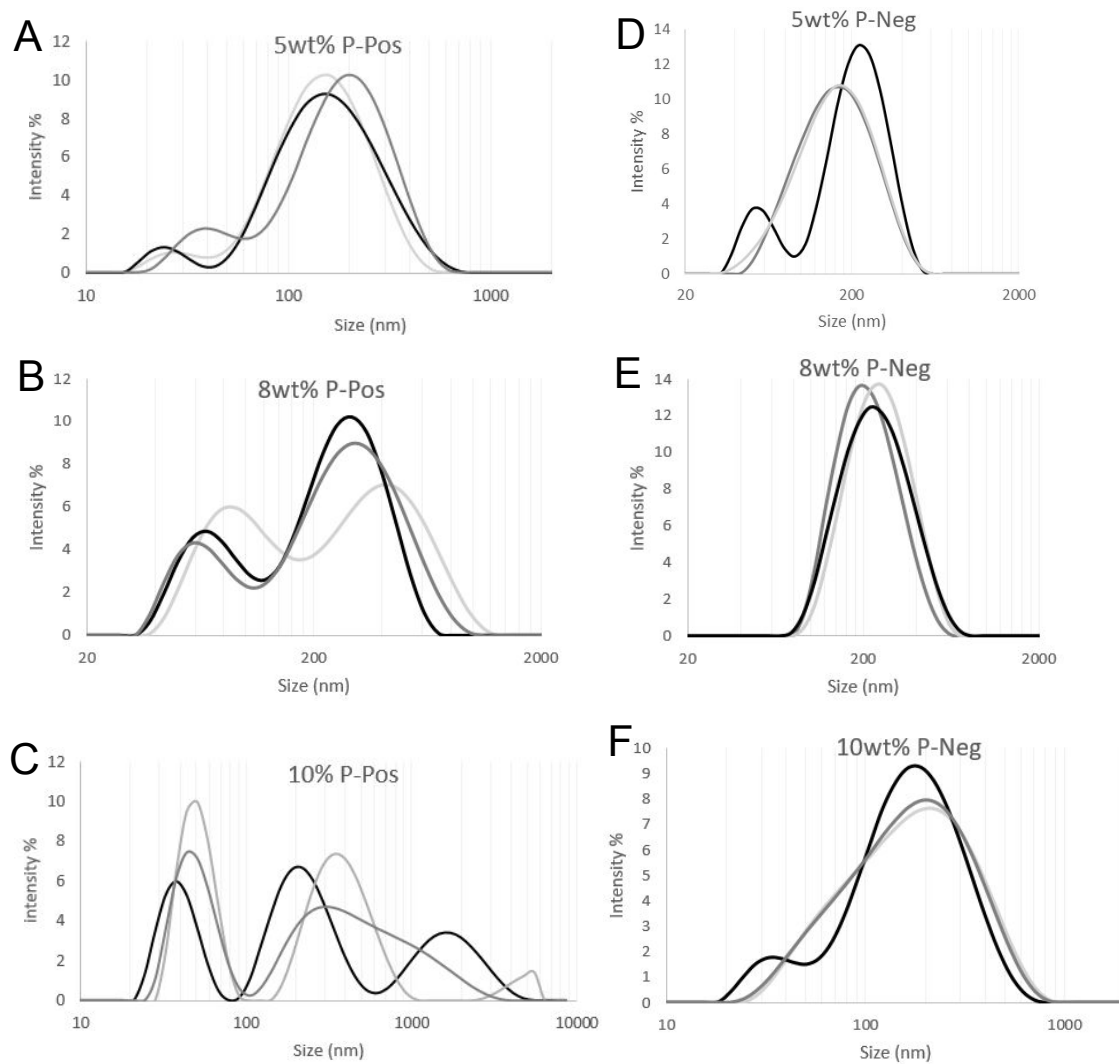




**Supplementary Figure 11.** Asymmetric Flow Field-Flow Fractionation (AF4) data for surface charge effect on formulation 6 recording the shape factor ( $\rho = R_g/R_h$ ) using in-line multi-angle light scattering (MALS) and DLS. (A) 5wt% P42-PCT(+) , (B) 8wt% P42-PCT(+), (C) 5wt% P42-PCT(-) , (D) 8wt% P42-PCT(-), (E) 10wt% P42-PCT(-) doped nanoworms. Shape factors overlap (F) Positively charged nanoworms: Black= 5wt%, Red= 8wt%, (G) Negatively charged nanoworms: Black= 5wt%, Red= 8wt%, Blue= 10wt%.



**Supplementary Figure 12.** Size distribution by intensity (DLS) data for surface charge effect on formulation 6. (A) 5wt% P42-PCT(+) , (B) 8wt% P42-PCT(+), (C) 5wt% P42-PCT(-) , (D) 5wt% P42-PCT(-), (E) 8wt% P42-PCT(-), (F) 10wt% P42-PCT(-) doped nanoworms.



**Supplementary Figure 13.** Dexamethasone UV/vis absorption spectra of 12 wt% loaded nanoworms (plain) and equivalent reference sample (dash).

